Supplementary information

A fuzzy-to-ordered switch of the binding mode in the disordered regulator HigA2 mediates a functional ratio-sensing gene circuit

Zala Živič[a], Tadej Medved[a,b], Zala Urbič[a], Luka Lipoglavšek[c], Remy Loris[d,e] Jurij Lah[a], San Hadži[a],

[a]*Department of Physical Chemistry, Faculty of Chemistry and Chemical Technology, University of Ljubljana, 1000 Ljubljana, Slovenia*

[b]*Novartis*

[c]*Department of Microbiology, Biotechnical Faculty, University of Ljubljana, 1000 Ljubljana, Slovenia*

[d]*Structural Biology Brussels, Department of Biotechnology, Vrije Universiteit Brussel, Pleinlaan 2, B-1050 Brussel,Belgium*

[e]*VIB Centre for Structural Biology, VIB, Pleinlaan 2, 1050 Brussels, Belgium*

Table of contents

Materials and methods

Bacterial strains and plasmids. All oligonucleotides (see

Table S5) and chemicals were purchased from Sigma-Aldrich. All relevant DNA sequences of inserts are accessible in **supplementary file SI DNA sequences.** Gene sequences of protein-coding *higBA2*, $higBA2_{110A}$, $higBA2_{110B}$, $higBA2_{110C}$ and $higBA2_{[3+][3-]}$ were chemically synthesized and cloned into pET15b expression vector using *Nde*I and *BamH*I restriction sites by a commercial supplier (Genscript). In these constructs, a cleavable histidine tag is placed at the protein N-terminus of toxin HigB2 while antitoxin HigA2 remains untagged. Gene sequences corresponding to *higA2* and $higA2_{[3+][3-]}$ were chemically synthesized and cloned into pet21b vector using NdeI and XhoI restriction site by a commercial supplier (Genscript). In these constructs an un-cleavable histidine tag is placed at the protein C-terminus. For amino acid sequences of all studied proteins see

Table S2. Slowest nontrivial normal modes of HigB2-HigA2 as obtained from an anisotropic network model of the C_α-atoms comprising the V-shaped conformation of HigB2-HigA2. The modes are sorted by ascending frequency. The squared overlap denotes the degree of similarity to the conformational change between the V-shaped and open conformations.

normal mode	frequency	squared overlap
7	0.23	0.508
8	0.30	0.001
9	0.34	0.000
10	0.60	0.000
11	0.61	0.013
12	0.76	0.006
13	0.80	0.000
14	0.98	0.000
15	1.02	0.000
16	1.11	0.000
17	1.22	0.000

Table S3**.**

For the *in vivo* reporter system with constitutive gene expression, we used the pSB1A3 vector harbouring the red fluorescent protein mRFP1 under the P_{higBA2} promotor (vector pSB1A3-PhigBA2-RFP). Gene fragments containing *higA2*, $higB2_{NA2}$ and *higB2*/*higA2* with the upstream constitutive promotor P_{117} from the Anderson promotor library (BioBrick identifier BBa_J23117)[1] were then ordered from a commercial supplier (Genscript). These fragments were inserted into the pSB1A3-PhigBA2-RFP using *Nde*I and *Pst*I sites. All constructs were verified by gene sequencing using oligonucleotides pSB1A3-F and pSB1A3-R (see

Table S2. Slowest nontrivial normal modes of HigB2-HigA2 as obtained from an anisotropic network model of the C_α-atoms comprising the V-shaped conformation of HigB2-HigA2. The modes are sorted by ascending frequency. The squared overlap denotes the degree of similarity to the conformational change between the V-shaped and open conformations.

normal mode	frequency	squared overlap
7	0.23	0.508
8	0.30	0.001
9	0.34	0.000
10	0.60	0.000
11	0.61	0.013
12	0.76	0.006
13	0.80	0.000
14	0.98	0.000
15	1.02	0.000
16	1.11	0.000
17	1.22	0.000

Table S3).

Inducible expression systems were based on the pRAT-sfGFP expression system.[2] Toxin gene was placed under control of arabinose-inducible P_{BAD}, antitoxin gene was placed under IPTG-inducible P_{T7} *lacO* and toxin-antitoxin system promoter was placed preceding reporter gene encoding for Superfolder

GFP (*sfGFP*). Golden Gate cloning method[3,4] using type II *Bsa*I enzyme was used to insert fragment containing P_{CP8} *araE* through a single pair of homology regions (HR7/8, see **Table S6**) into pRAT-sfGFP-HigBA2. The plasmid bearing insert (pET21b(+)-PCP8-araE) and the destination plasmid (pRAT-sfGFP-HigBA2) were synthesized and provided by a commercial supplier (Twist Bioscience). For the study of antitoxin HigA2 point mutations and the modification of *higB2* into *higB2* with new and altered D-loop we used oligonucleotides (see

Table S5) in order to perform cloning through *In vivo assembly* (IVA).[5] PCR-amplified mutant DNA was transformed into XL1Blue(INOUE)[6] following *Dpn*I digestion of matrix DNA. Oligonucleotides AraE-N-F, SEQ-T7-lac, SEQ-PBAD and SEQ-15a-ORI were used to validate sequences of *araE*, antitoxin, toxin and toxin-antitoxin system promoter preceding *sfGFP*, respectively.

Protein purification. Constructs bearing His-tagged *higBA2*, *higA2* and their variants were transformed into BL21[DE3] cells. Single colonies were inoculated into 10-30 mL of LBA and grown overnight at 37°C, 120 rpm. Overnight cultures were diluted into fresh LBA at a ratio of 1:50 with a final volume of up to 1.2 L. Cells were grown at 37°C, 120 rpm to an approximate OD_{600} of 0.6-0.8 at which point 1 mM of IPTG was added to induce gene expression. Following 3-4 hours of induction at 37°C, 120 rpm, the cells were harvested by centrifugation for 20 min at 4000 g. Supernatant was discarded and pellet was resuspended in Lysis Buffer (20 mM Tris, 0.5 M NaCl, pH = 8, cOmplete Ultra tablets, EDTA-free (Merck)). Cells were sonicated for 5 min (amplitude = 40, frequency = 0.4 s) on ice using Ultrasonicator UP100H (Hielscher). Following 30 min centrifugation at 14 000 g, soluble phase was filtered through 0.2 μm filter (Sartorius). Ni-affinity chromatography was then performed using Akta Purifier (Cytiva) on His-Trap HP column (5 mL, Cytiva).

For the purification of His-tagged antitoxin and toxin-antitoxin complexes, column was washed using Binding Buffer (20 mM Tris, 0.5 M NaCl, pH = 8) following soluble phase application. Bound protein was eluted using a gradient or step additions of Elution Buffer (20 mM Tris, 200 mM NaCl, 1 M imidazole, pH = 8). When the purification of untagged antitoxin and its variant was desired, an on-column unfolding/refolding protocol was performed.[7] Sample-loaded column was washed with 4 column volumes (CV) of Wash buffer (20 mM Tris, 1 M NaCl, 10 % (V/V) ethylene glycol), pH = 8). Then, denaturation was performed in two steps with 4 CV of 50 % and then 4 CV of 100% of Denaturation buffer (20 mM Tris, 0.5 M NaCl, 5 M Ganidinium chloride, pH = 8). Refolding was initiated with 4 CV of Refolding buffer 1 (20 mM Tris, 25 mM NaCl, 5 % (V/V) glycerol, pH = 8) and another 4 CV of Refolding buffer 2 (20 mM Tris, 25 mM NaCl, 1 % (V/V) glycerol, pH = 8), followed by gradient elution using Elution Buffer (20 mM Tris, 200 mM NaCl, 1 M imidazole, pH = 8). In the case of HigB2-HigA2, both toxin and antitoxin remain bound to column until elution, with antitoxin being eluted at very low percentages of Elution buffer (~5 %).

Samples gathered following Ni-affinity chromatography were diluted at least 10-fold into final Sample buffer (20 mM Tris, 150 mM NaCl, pH = 8) and then concentrated using Amicon Ultra (15 mL, MWCO 3/10 kDa, Merck) to ~500 μL for Size-exclusion Chromatography (SEC) on Superdex 75 GL column (Cytiva) using Akta Purifier (Cytiva). Fractions following Ni-affinity chromatography and SEC were assessed using SDS-PAGE (see **Figure S11**). Protein concentration and purity was assessed using Nano Spectrophotometer (VWR) measurements at A_{280}. Fractions containing pure protein were concentrated using Amicon Ultra (15 mL, MWCO 3/10 kDa, Merck) and stored at -20 °C for further use.

Promoter activity *in vivo*. For experiments involving promoter activity in *E. coli*, two approaches were used. The first involved expressing toxin-antitoxin genes constitutively. Vectors pSB1A3 harbouring *higBA2* genes and their variants were transformed into competent BL21[DE3] cells. Overnight cultures were grown in 6 mL LBA at 37 °C with constant shaking at 120 rpm. Cultures were then diluted into fresh LBA media (0.3 mL) at a ratio of 1:50 and further incubated at 30 °C with constant shaking in 48-well Nunclon flat bottom plates in Synergy H1 (Agilent). OD_{600} and fluorescence intensity measurements (λ_{ex} = 580 nm λ_{em} = 620 nm) were measured following 20 h of growth. Promotor activity (P_A) was determined by normalizing the fluorescence intensity (*FL*) corrected for the change in OD_{600} at time of measurement (*t*) as depicted in ***Equation 1***.

$$P_A = \frac{FL(t)}{t*(OD_{600}(t)-OD_{600}(t=0))} \qquad \textbf{\textit{Equation 1}}$$

The second approach involved inducible promoters P_{BAD} (toxin gene expression) and P_{T7} *lacO* (antitoxin gene expression). Plasmids containing toxin-antitoxin system were transformed into Tuner[DE3] cells. Overnight cultures grown in 2 mL minimal media M9K (see

Table S7) were diluted into fresh M9K 1:20 (up to 6 mL) and grown overnight at 18 °C, 135 rpm. Following this, the cells were induced using IPTG and/or L-arabinose at appropriate concentrations in 100 μL aliquots in Greiner CELLSTAR® 96 well plates using plate reader Synergy H1 (Agilent). Growth and reporter protein production was measured each for up to 48 h by measuring OD_{600} and Fluorescence (λ_{ex} = 483 nm λ_{em} = 535 nm). For experiments with delayed addition of L-arabinose, cells were grown only in the presence of IPTG for the first 20 h, following which L-arabinose was added to plates and growth monitoring resumed. Fluorescence measurements were normalized against OD_{600}.

Flow cytometry measurements. Cells containing the appropriate vectors were inoculated into overnight culture and grown in 5 mL LBA (constitutive promoters) or in 2 mL M9K (inducible promoters) at 37 °C with constant shaking. Overnight culture was diluted into 5 mL of fresh media and grown for 20 h prior to single cell fluorescence measurements (constitutive promoters). For inducible promoters, cells were grown and induced for 20 h as described above. Cells were diluted to concentrations of approximately 10^8 cells/mL in phosphate buffer solution (1× PBS, cells diluted 500-4000x) and measured using FACScan flow cytometer (Becton Dickinson) with a 488 nm excitation laser. Around 30000–32000 events were collected at speeds up to 2000 events/second. Flow cytometer measured forward scatter (FSC), side scatter (SSC) and fluorescence data (530/30 nm and 650 LP). Data was analysed using Flowing Software 2 (Turku Bioscience). Fluorescence data was gated as depicted in supplementary material (see **Figure S8**).

Electrophoretic mobility shift assay (EMSA). For EMSA experiments, Cy-5-labelled DNA (see

Table S5) was annealed at a ratio of 1:1 (forward:reverse) at 90 °C and cooled to room temperature slowly. Samples containing appropriate concentrations of DNA and proteins were pre-incubated for 1 h at room temperature prior to application to Native PAGE gel. Sample volume was 12 µL, which included 3 µL of 4x Native PAGE L.B. (125 mM Tris, 50 % glycerol (V/V), 0.1 % Bromphenol Blue (w/V), pH = 8.8), 0.5 µM (when studying HigB2-HigA2 complexes)/0.15 µM (when studying HigA2 dimers) annealed DNA-Cy5, appropriate concentrations of proteins, 2 µM non-target DNA (calf thymus extract) and appropriate amounts of Sample buffer (20 mM Tris, 150 mM NaCl, pH = 8). For the study of tetramer-DNA interactions 7 % gels were used, whereas antitoxin-DNA interactions were monitored using a 10 % gel. Electrophoresis was performed in 1xTAE buffer (40 mM Tris, 1 mM EDTA, 8 mM acetic acid) at 120 V and 100 mA for 1 h. DNA-visualization was performed using imager ChemiDoc MP (BioRad) at excitation and emission wavelengths of Cy5 (700/50, Red Epi).

Western Blot. For the purposes of toxin and antitoxin detection, proteins were purified from 50 mL of Tuner[DE3] cells grown in minimal media M9K in the presence of appropriate amounts of inducer for 8-10 h. Proteins were purified using anti-His magnetic beads His Mag Sepharose Ni (Cytiva). Antitoxin purification included an added pre-incubation step with 8 µg of His-tagged toxin. Purified proteins were separated on SDS-PAGE gel (15 %), following which protein transfer was performed onto nitrocellulose membrane (Cytiva, 0.2 µm pore size) in Towbin transfer buffer (25 mM Tris, 192 mM glycine, 20 % methanol, pH = 8.2) using Trans-Blot Turbo System (BioRad) for 7 min at 1.3 A and 25 V (MIXED MW setting, 1 mini gel). Membrane was then blocked using Blocking buffer (1xPBST, 5 % skim milk) or 30 min at room temperature with constant gentle rocking. Following that, we washed the membrane in Wash buffer (1x PBST) 3-times for 5 minutes. Membrane was then incubated overnight in 10 mL of 1xPBST with 1 µg/mL monoclonal mouse anti-His (MediMabs) or monoclonal mouse anti-HA (Biosensis) primary antibody in sterile 50 mL centrifuge tubes with constant rolling. After another 3-washing steps, the membrane was incubated for 1 h in 10 mL of 1xPBST with 0.2 µg/mL polyclonal HRP-conjugated goat anti-mouse secondary antibody (ImmunoReagents) in sterile 50 mL centrifuge tubes with constant rolling. Following final 3 wash steps, membrane was gently dried and HRP-substrate 1-step ULTRA TMB (Pierce) was added. Substrate and membrane were incubated for up to 30 min, after which substrate was gently removed and membrane was photographed using imager ChemiDoc MP (BioRad).

Anisotropy measurements. Protein samples were prepared as 10 µM, 1 µM and 0.1 µM stock and titrated into annealed 100 nM or 20 nM of DNA 45-Cy5 (see

Table S5) with 14-18 additions in total and incubated 3-10 min at room temperature. Anisotropy measurements were performed at λ_{ex} = 633 nm and λ_{em} = 662 nm, with 5 nm of excitation bandwidth and 10 nm emission bandwidth, high sensitivity and 5 accumulations at 20 °C. Data was exported and several datasets were fitted with a model function Δr_m (***Equation 2***) by varying constants of dilutive effect (Δr_0), maximum anisotropy effect upon full binding (Δr_{max}) and the constant of dissociation (K_D).[8]

$$\Delta r_m = \Delta r_0 + \frac{(\Delta r_{max} - \Delta r_0) * c(protein)}{c(protein) * K_D} \qquad \textbf{Equation 2}$$

Concentration of protein (*c(protein)*) was accounted for to provide an optimized fit. It was determined as the concentration of tetramer complex for the titration of tetrameric HigB2-HigA2 and its variants into DNA (*c(protein)* = c(tetramer)), whereas for antitoxin HigA2, concentration of protein was determined as dimer concentration ((*c(protein)* = c(dimer)). Data and model function was then presented as percentages between minimum (0 set at Δr_0) and maximum (1 set at Δr_{max}) values for clarity.

Isothermal calorimetry (ITC). Purified proteins and annealed unlabelled DNA were dialysed using 0.5-3 mL Slide-A-Lyzer 3.5 MWCO Dialysis Cassette (ThermoFisher Scientific) against 2-volumes of Sample buffer (~1 L, 20 mM Tris, 150 mM NaCl, pH = 8) for 3 hours at room temperature and then overnight against 2 L of Sample buffer at room temperature. Magnetic stirrer provided constant gentle mixing. Protein concentration and purity was assessed using Nano Spectrophotometer (VWR) measurements at A_{280}. ITC experiments were performed using Microcal PEAQ-ITC isothermal titration calorimeter (Malvern Instruments, Malvern Panalytical Ltd) at 25 °C. Antitoxin variants or tetramer variants were titrated into solution containing DNA. Antitoxin variants were also titrated into solution containing toxin. 19 injections of initial concentration of protein complex (32 μM antitoxin dimer (for toxin binding), 37.25 μM antitoxin dimer (for DNA binding) and 127.5 μM toxin-antitoxin tetramer) were added to ligand (10 μM annealed DNA for tetramer, 2 μM DNA for antitoxin dimer and 5 μM of toxin monomer). Reference power was 10.0 μcal s−1, feedback was set to high and stir speed was 750. Data was exported and integrated using program NITPIC (version 2.1.0)[9] and analysed with SEDPHAT (version 15.2).[10] Monte-Carlo approach was used for parameter and error analysis in SEDPHAT.

Crystallography. Crystallization and data collection of the HigB2-HigA2-operator complex has been reported previously.[11,12] Purified protein complexes of HigB2-HigA2A_{110A}, HigB2-HigA2A_{110B} and of HigB2-HigA2A_{110C} (~ 5 mg/mL) were applied in 0.2 μL to 0.2 μL of several screening solutions and subjected to crystallisation trials using drop vapor diffusion against 55 μL of reservoir solution. Following several weeks, crystals of HigB2-HigA2A_{110A} grew in 0.2 M ammonium nitrate, 20 % PEG 3350 and were harvested in the presence of 30 % (V/V) of glycerol added as a cryoprotectant. Data collection was performed at SOLEIL synchrotron beamline Proxima-1 and the collected data was indexed, scaled and integrated using XDS. Structure of the HigB2-HigA2-operator complex was solved using molecular replacement in PHASER using the HigB2-HigA2$_{2\text{-}33}$ (from PDBID: 5JAA) complex as search model. The resulting electron density clearly showed the presence of DNA molecule, which was then built manually in Coot.[13] Structure of HigB2-HigA2A_{110A} was solved using molecular replacement in PHASER using individual HigB2 and HigA2 structures (from PDBID: 5JAA) as search models. Both structures were then subjected to several rounds of model building and refinement in phenix.refine.[14] For HigB2-HigA2A_{110A} final refinement steps included TLS refinement, one chain per group. For HigB2-HigA2-operator data was of lower resolution therefore refinement included restraints from the high-resolution reference models (HigA2-operator, PDBID: 8A0W), NCS restraints and secondary structure restraints as implemented in phenix.refine.

Small-angle X-ray scattering. Purified protein (HigA2 or HigA2$_{[+][-]}$) and annealed unlabelled DNA (DNA33) was combined at a ratio of 1:1 and then concentrated using Amicon Ultra (15 mL, MWCO 3 kDa, Merck) to an approximate concentration of 0.3 mM in in 20 mM TRIS pH 8 and 200 mM sodium chloride. SAXS data were collected in the HPLC mode on the SWING beamline at the SOLEIL synchrotron (Gif-sur-Yvette, France). Samples were injected into a Shodex KW 402.5-4F column and

run at 0.2 ml/min. Data was processed with Foxtrot[15] and programs from the ATSAS package: OLIGOMER, GNOM and PRIMUS.[16]

Normal mode analysis of HigB2-HigA2 conformational flexibility. The geometric contribution to the conformational flexibility of the HigB2-HigA2 tetramer was assessed via normal mode analysis using the ProDy Python library.[17] Briefly, an anisotropic network model of the HigB2-HigA2 C_α-atoms was built with default parameters, and the 10 lowest-frequency nontrivial normal modes were extracted (see **Table S2**). The most biologically relevant normal modes were determined by calculating the squared overlap between the eigenvector of each individual normal mode and the normalized deformation vector between the DNA-bound (PDBID: 8A0X) and unbound (PDBID: 5JAA) conformations. The lowest-frequency normal mode is depicted in **Movie S1**.

Protein design of HigA2 globular domain with enhanced DNA binding. The crystal structure of the HigB2-HigA2 tetramer in complex with *higBA* operator DNA (PDBID: 8A0X) was used as the template model, and was pre-processed by removing any crystal artifacts, as well as both HigB2 subunits and the disordered N-terminus of each half of the HigA2 dimer (residues 1-36). The design space was comprised of interface residues between the HigA2 C-terminal dimer and DNA (heavy-atom distance cutoff ≤ 5 Å). Interface residues within the distance cutoff of any nucleobase were removed from the design space in order to preserve specificity. Additionally, residues Glu37 and Val46 were considered despite a greater distance from the DNA backbone, as a theoretical mutation to Arg or Lys could bring them within the distance cutoff for interaction. Potential mutations were proposed based on LigandMPNN[18] model probabilities. The model weights *ligandmpnn_v_32_010_25* (training data with 0.10 Å Gaussian noise) were used, and for each designable position, probabilities for all 20 amino acid identities were estimated under the autoregressive scheme with sequence context. The probabilities were averaged across 50 separate batches, and potential mutations were selected based on a minimum cutoff probability of 0.05, averaged across equivalent chains.

The suitability of the proposed mutations was assessed *in silico* by generating 50 refined models for each mutant sequence with the Rosetta macromolecular modelling suite (version 3.13)[19] and averaging the computed binding energies. A custom RosettaScripts[20] protocol was used to assess the impact of point mutations on the theoretical binding energy of the HigA2 C-terminal domain to target DNA, and was run within the RosettaDNA application.[21–23] First, each set of mutant residues was threaded onto the template structure with *PackRotamersMover*. Then, *DnaInterfacePacker* was used to repack and minimize the side chains on the protein side of the interface with all DNA atoms held fixed. The *RestrictDesignToProteinDNAInterface* task operation was used to restrict packing and minimization to all residues within a distance of 3 Å from the closest DNA atom. *DnaInterfacePacker* was also used to calculate the binding energy as the difference in scores between the relaxed complex and the sum of the unbound protein and DNA following a separation of 1000 Å. The DFPMIN-Armijo algorithm was used for energy minimization at a tolerance threshold of 1e-4. All scoring was performed with the *dna* energy function.[23] Mutations that increased the binding energy by ≥ 5 REU were removed from consideration.

Protein design of HigB2-HigA2 tetramer variants. In order to generate HigB2 and HigA2 sequences likelier to fold into the stable **V-shaped** conformation in the *apo* state, we formulated a custom design algorithm incorporating both positive and negative design principles (**Figure S2**). The crystal structures of the DNA-bound conformation (PDBID: 8A0X – **positive template**) and the wild-type *apo* conformation (PDBID: 5JAA – **negative template**) were used as starting points. Both templates were pre-processed by removing all co-crystallized waters, ions, crystallization reagents, and DNA in the case of the positive template. Additionally, all selenomethionine residues found in the negative template were replaced with methionines in ChimeraX using the DockPrep application.[24] Finally, missing density corresponding to a disordered loop in the HigB2 subunits (residues 52-63) in the negative template was addressed by grafting equivalent loops that were fully structured in the positive template. In brief, each of the HigB2 subunits from the positive template was superimposed onto the corresponding HigB2 subunit in the negative template by minimizing their backbone RMSD. The two disordered loops

(residues 52-63) were then manually grafted onto the negative template, which was subsequently input to the Rosetta Loopmodel application, using the Kinematic Closure (KIC) algorithm to repair potential chain breaks.[25] The lowest-energy conformation (out of 100 total) was selected as the new negative template. The positive and negative templates were then each subjected to full-atom relaxation using a custom RosettaScripts protocol. Briefly, all surface residue sidechains (with absolute SASA > 40 Å^2) were first repacked, followed by energy minimization of all sidechains in the template. This was repeated twice, then all sidechains were repacked a final time before minimization of all sidechain and backbone atoms in the structure. For packing, input sidechain rotamers were considered and extra rotamers were sampled around the χ_1 and χ_2 angles, however the χ_2 angle was constrained between 70° and 110° for all aromatic residues. Energy minimization was performed using the nonmonotone L-BFGS-Armijo algorithm with a tolerance threshold of 1e-3. The *beta_nov16* energy function with Cartesian weights was used throughout the protocol.[26] 100 relaxed structures were generated for each template.

The crystal structure of the positive template (PDBID: 8A0X) was used to define the residue design space. First, per-residue SASA was calculated via NACCESS[27] with default parameters for both the complex structure and the individual subunits, with only the C-terminal domain (residues 37-104) taken into consideration in the case of HigA2. All residues across the HigB2-HigA2 interface with at least one heavy-atom pair within a distance ≤ 5 Å and with a per-residue ΔSASA ≥ 50 Å^2 were designated as interacting residues. Any residues found to be at the interface with the bound DNA (heavy-atom pair distance ≤ 5 Å and residue ΔSASA ≥ 50 Å^2) were excluded. This exercise was performed for both HigB2-HigA2 interfaces (chains A-C and B-D in the positive template), and the final design space was set as the union of interacting residue positions found at either interface.

To reduce the number of potential sequences, the inverse folding model ProteinMPNN[28] was used. First, a pair of positive and negative templates was selected from the lowest-scoring relaxed sets. ProteinMPNN with model parameters *proteinmpnn_v_48_020* (training data with 0.20 Å Gaussian noise) was then applied to the positive template to generate a single batch of 50 unique sequences with sampling temperature T = 0.3. Equal symmetry weights were set for all designable residues in both HigB2-HigA2 interfaces. Mutations to Cys or Pro were forbidden, while all other amino acid identities retained equal bias. The obtained mutant sequences were threaded onto both the positive and negative templates with the Rosetta *PackRotamersMover*, then both models were relaxed using the same protocol as above. This was repeated 20 times for each sequence, and all subsequent Rosetta scores were averaged across the 20 mutant models.

$$\Delta E_{wt} = \bar{E}^{mut}_{positive\ model} - \bar{E}^{wt}_{positive\ model} \qquad \textbf{Equation 3}$$

$$\Delta E_{mut} = \bar{E}^{mut}_{positive\ model} - \bar{E}^{mut}_{negative\ model} \qquad \textbf{Equation 4}$$

$$F = w_1 \Delta E_{wt} + w_2 \Delta E_{mut} \qquad \textbf{Equation 5}$$

The 50 mutant sequences were ranked according to a custom scoring function, with the objective to maximize the Rosetta energy difference between the positive mutant and wild-type models (***Equation 3),*** as well as the positive and negative mutant models (***Equation 4***). The two terms were then weighted and summed to obtain the final objective function (***Equation 5***) with weights w_1 = 1.0 and w_2 = 2.0. Once ranked by increasing objective function value, the top 25 sequences were retained. To account for any noise generated during the relaxation of the positive and negative models, the above workflow was repeated for the 3 lowest-scoring pairs of relaxed positive and negative template conformations, netting a pooled set of 75 unique sequences. These were subjected to additional filtering, first by removing any mutants with $\Delta E_{mut} > 0$. Secondly, we obtained predicted models for our mutant sequences using the AlphaFold3 server.[29] The proposed sequences were ranked according to the average full-structure pLDDT score and Cα-RMSD from the positive template crystal structure aligned on the HigA2 C-

terminal domain (residues 37-104). All scores were averaged across 5 diffusion samples obtained from a single seed. The top 3 sequences were used for experimental characterization.

Steady-state (equilibrium) model of *higBA2* circuit. The equilibrium model of the *higBA2* system was devised similarly as for the *ccdBA* module reported previously (**Figure S12**).[30] Three mass-balance equations corresponding to total concentration of toxin, antitoxin and operator DNA were expressed as the sums of stoichiometrically-weighted concentrations of their protein-protein or protein-DNA complexes. The concentration of each macromolecular complex can be further expressed as a product of free reactant concentrations (toxin, antitoxin, DNA) weighted by the respective equilibrium constants (K_{TA}= 2.0e+11 ; K_{AD}=2.0e+08 ; K_{TAD}=2.0e+06, for HigB2-HigA2, HigA2-DNA and HigB2-HigA2:DNA complexes, respectively). This results in three sets of nonlinear equations which were used to calculate the concentrations of reactants (free toxin, antitoxin, DNA) given their total concentration. This was achieved using root solving *fsolve* routine from the scipy.optimize package. For the calculation of operator occupancy (concentration of free operator divided by total operator concentration) a fixed concentration of DNA operator was assumed (c_{DNA}=1 nM) and different total concentrations of toxin and antitoxin, as indicated in the figures.

Stochastic kinetic simulations. The general layout of the four toxin-antitoxin regulatory circuits is shown in **Figure S12**. In all systems, we accounted for both the formation of the TA complex and the TAT complex. As species, we thus defined mRNA, antitoxin (A), toxin (T), both complexes (TA, TAT), and the level of free operator (D). As can be seen from **Figure S12**, in the system with conditional cooperative regulation (conditional cooperativity), repression occurs through the TA complex, while in the system with anti-cooperative regulation (anti-conditional cooperativity), repression occurs only through protein A. In the system with negative regulation, both protein A and both complexes (TA and TAT) bind to the operator, whereas in the system without regulation, no species binds to the operator. For the stochastic simulations we modified a publicly available code from Caltech (Stochastic simulation of biological circuits).[31] Core parameter values were taken form the study.[32] which addressed the performance of conditional cooperativity in phd/doc module. In order for the systems to be comparable it is necessary to achieve same steady-state concentrations of total toxin and antitoxin. We therefore used the same core set of parameters throughout (see **Table S8**), with few adjustments of parameters values to achieve same steady-state level as in the system with conditional cooperative regulation. In particular, for the system without regulation mRNA production was reduced by factor 5.02 **(ζ/ 2.24 and dm *2.24)**, while for the systems with anti-cooperative regulation we either reduced the level of repression (***αA*/1.28 and *θA**1.28)** or increased mRNA production (**ζ*1.19 and dm/1.19**). Similar modification was also used in system with negative regulation (**ζ*1.81 and dm/1.81 or *αA*/2.05 and *θA*2.05).***

The general outline of simulation with **change of parameters has been described before**[33] and allows comparisons of the system's performance in terms of recovery dynamics from the persistent state. To improve statistical analysis, we repeated the simulations 1000 times. For the recovery dynamics from the persistent state, we first simulated the systems for some time with normal parameter values, then switched to a new set of parameters (**Table S8**, column "Changed parameters") for some time, which represent bacterial starvation conditions, and finally switched back to the initial conditions, as described in the article. Under starvation conditions, we considered that translation slows down (by 10-fold) due to amino acid deficiency, cells divide more slowly, which slows down the reduction in protein concentration due to dilution (by 10-fold), and additionally, the Lon protease is activated, which begins to degrade both free antitoxin and antitoxin within complexes 8 times faster. For the transition to the persistent state to be sufficiently rapid, it is important that antitoxin within complexes is also degraded, which is expected to degrade approximately 4 times slower. Furthermore, we included in the simulation the toxic effect of the toxin in terms of degradation of mRNA encoding the toxin and antitoxin. However, we did not account for the toxin also degrading other mRNAs in the cell.

Given that a different set of parameters was used in the article, we did not use the same value for the mRNA degradation constant, as it would be too large and the system would take too long to recover

from the persistent state. We reduced the constant enough so that the average mRNA level in all systems in the persistent state dropped just below 1. Recovery to the steady state is a complex process dependent both on the degradation of the toxin itself before the mRNA level rises again, as well as sequestration into complexes when new antitoxin begins to form. Because of this, we could not analyse the recovery in terms of kinetics and assign a specific order to the curve. Given that at least initially the curves are quite similar to straight lines, for each simulation replicate we fitted a straight line to the curve from the peak to a toxin value of 10 and determined its slope, which corresponds to the system's return constant k as depicted on the **Figure 6**.

To calculate the vector Fields of TA systems we performed the simulation with the same parameters, except that we carried out the simulation for five binding sites on the operator. For all three regulatory systems (conditional cooperative regulation, anti-cooperative regulation, negative regulation), we performed simulations starting with different Ttot:Atot ratios and then ran the simulation long enough to establish a steady state. First, we kept the initial Ttot at a value of 1800 molecules and changed the initial Atot in increments of 100 from 100 to 1500, then we kept Atot at a value of 100 molecules and changed Ttot from 100 to 1800. Then, for all three systems, we plotted Ttot versus Atot graphs with arrows for all simulation replicates, where the length of individual arrows represented the rate of change of Atot and Ttot in the system.

Supplementary Tables

Table S1. Crystallography data for the structural determination of HigB2-HigA2 complexes.

	HigB2-HigA2-110A	HigB2ΔHis-HigA2-Opr31$_{C/G}$
PDB code	9TV9	8A0X
Diffraction source	SOLEIL synchrotron, Proxima I	SOLEIL synchrotron, Proxima IIA
Wavelength (Å)	0.978565	0.98010
Temperature (K)	100	100
Detector	PILATUS 6M	ADSC Q315r
Crystal-detector distance (mm)	297.28	429.00
Rotation range per image (°)	0.1	0.5
Total rotation range (°)	360	90
Space group	C2	$P4_12_12$
a, b, c (Å)	112.1, 73.7, 77.8	113.6, 113.6, 121.1
α, β, γ (°)	90, 131.7, 90	90, 90, 90
Mosaicity (°)	0.097	0.218
Resolution range (Å)	49.26-2.00 (2.12-2.00)	48.30 - 3.30 (3.49-3.30)
Total No. of reflections	224588 (36466)	86951 (13618)
No. of unique reflections	31631 (5017)	12408 (1921)
Completeness (%)	98.0 (97.2)	99.3 (98.6)
Redundancy	7.1 (7.2)	7.0 (7.1)
〈 I/σ(I)〉	9.39 (1.23)	12.3 (2.0)
$R_{r.i.m.}$ / R_{merge}	0.127 (1.289)	0.187 (1.23)
CC1/2	99.8 (76.4)	99.7 (73.2)
Overall B factor from Wilson plot (Å^2)	37.7	95.8
R-work	0.2260 (0.3865)	0.1970 (0.3358)
R-free	0.2501 (0.4076)	0.2561 (0.4045)
Number of non-hydrogen atoms	3514	4601
macromolecules	3345	4601
ligands	42	0
water	127	0
Protein residues	415	486
RMS(bonds)	0.015	0.007
RMS(angles)	1.43	1.07
Ramachandran favored (%)	98.27	98
Ramachandran allowed (%)	1.73	
Ramachandran outliers (%)	0	0
Clashscore	4.48	11.63
Average B-factor	58.72	107.20
Macromolecules	59.02	107.20
Ions	70.28	/
Solvent	46.91	/

Table S2. Slowest nontrivial normal modes of HigB2-HigA2 as obtained from an anisotropic network model of the C_α-atoms comprising the V-shaped conformation of HigB2-HigA2. The modes are sorted by ascending frequency. The squared overlap denotes the degree of similarity to the conformational change between the V-shaped and open conformations.

normal mode	frequency	squared overlap
7	0.23	0.508
8	0.30	0.001
9	0.34	0.000
10	0.60	0.000
11	0.61	0.013
12	0.76	0.006
13	0.80	0.000
14	0.98	0.000
15	1.02	0.000
16	1.11	0.000
17	1.22	0.000

Table S3. Amino acid sequences of proteins studied in this work.

Name	Sequence
HigA2(*wt*)-His	MSNRDLFAELSSALVEAKQHSEGKLTLKTHHVNDVGELNISPDEIVSIREQFNMSRGVFARLLHTSSRTLENWE QGRSVPNGQAVTLLKLVQRHPETLSHIAELLEHHHHHH*
HigA2$_{[3+][3-]}$-His	MSNRDLFAELSSALVEAKQHSEGELELKEHHVNDVGRLNISPDEIRSIREQFNMSRGVFARLLHTSSRTLENW EQGRNVPNGQAVTLLKLVQRHPETLSHIAELLEHHHHHH*
HigB2(*wt*)	MKSVFVESTIFEKYRDEYLSDEEYRLFQAELMLNPKLGDVIQGTGGLRKIRVASKGKGKRGGSRIIYYFLDEKR RFYLLTIYGKNEMSDLNANQRKQLMAFMEAWRNEQS
HigB2$_{R64A\ K84A}$	MKSVFVESTIFEKYRDEYLSDEEYRLFQAELMLNPKLGDVIQGTGGLRKIRVASKGKGKRGGSAIIYYFLDEKR RFYLLTIYGANEMSDLNANQRKQLMAFMEAWRNEQS
HigB2$_{Dloop}$	MKSVFVESTIFEKYRDEYLSDEEYRLFQAELMLNPKLGDVIQGTGGLRKIRVDDEEDDSAIIYYFLDEKRRFYL LTIYGANEMSDLNANQRKQLMAFMEAWRNEQS
HigB2$_{NA2}$	MSNRDLFAELSSALVEAKQHSEGKLTLKTHHVNDVGELNISGGGMKSVFVESTIFEKYRDEYLSDEEYRLF QAELMLNPKLGDVIQGTGGLRKIRVASKGKGKRGGSAIIYYFLDEKRRFYLLTIYGANEMSDLNANQRKQLM AFMEAWRNEQS
His-HigB2-HigA2 (*wt*)	MGSSHHHHHHSSGLVPRGSHMKSVFVESTIFEKYRDEYLSDEEYRLFQAELMLNPKLGDVIQGTGGLRKIRVA SKGKGKRGGSRIIYYFLDEKRRFYLLTIYGKNEMSDLNANQRKQLMAFMEAWRNEQS* MSNRDLFAELSSALVEAKQHSEGKLTLKTHHVNDVGELNISPDEIVSIREQFNMSRGVFARLLHTSSRTLENWE QGRSVPNGQAVTLLKLVQRHPETLSHIAEL*
His-HigB2-HigA2$_{[3+][3-]}$	MGSSHHHHHHSSGLVPRGSHMKSVFVESTIFEKYRDEYLSDEEYRLFQAELMLNPKLGDVIQGTGGLRKIRVA SKGKGKRGGSRIIYYFLDEKRRFYLLTIYGKNEMSDLNANQRKQLMAFMEAWRNEQS* MSNRDLFAELSSALVEAKQHSEGELELKEHHVNDVGRLNISPDEIRSIREQFNMSRGVFARLLHTSSRTLENW EQGRNVPNGQAVTLLKLVQRHPETLSHIAEL*
His-HigB2-HigA2$_{110A}$	MGSSHHHHHHSSGLVPRGSHMKSVFVESTIFEKYRDEYLSDEEYKLFQHKLALNPKLGDVIQGTGGLRKIRV ASKGKGKRGGSRIIYYFLDEKRRFYLLTIYGKNEMSDLNANQRKQLMAFMEAWRNEQS* MSNRDLFAELSSALVEAKQHSEGKLTLKTHHVNDVGELNISPDEIVSIRDSHNLSRGQFATLLHTSSRTLENWE QGRSVPNGQAVTLLKLVQRHPETLALIAEL*
His-HigB2-HigA2$_{110B}$	MGSSHHHHHHSSGLVPRGSHMKSVFVESTIFEKYRDEYLSDEEYRLFQHKLALNPKLGDVIQGTGGLRKIRVA SKGKGKRGGSRIIYYFLDEKRRFYLLTIYGKNEMSDLNANQRKQLMAFMEAWRNEQS* MSNRDLFAELSSALVEAKQHSEGKLTLKTHHVNDVGELNISPDEIVSIRDSFDLSRGIFAKLLHTSSRTLENWE QGRSVPNGQAVTLLKLVQRHPETLALIAEL*
His-HigB2-HigA2$_{110C}$	MGSSHHHHHHSSGLVPRGSHMKSVFVESTIFEKYRDEYLSDEEYRLFQHKLALNPKLGDVIQGTGGLRKIRVA SKGKGKRGGSRIIYYFLDEKRRFYLLTIYGKNEMSDLNANQRKQLMAFMEAWRNEQS* MSNRDLFAELSSALVEAKQHSEGKLTLKTHHVNDVGELNISPDEIVSIRDSYNLSRGQFATLLHTSSRTLENWE QGRSVPNGQAVTLLKLVQRHPETLARIAEL*

Antitoxin mutations increasing or decreasing HigA2-DNA binding affinity are depicted in orange and yellow, respectively.
Antitoxin N-terminus added to HigB2 is depicted in bold underlined blue letters.
Toxin and antitoxin mutations are depicted in bold pink and blue letters, respectively.
Linker regions are depicted in bold black letters.

Table S4. SAXS parameters

	HigB2ΔHis-HigA2	HigA2-DNA33	$HigA2_{[3+][3-]}$-DNA33
SASPDB accession code	SASDEV6	SASDER7	SASDEW6
Data collection			
Instrument		SOLEIL, SWING	
Wavelength (Å)		1.03	
q range ($Å^{-1}$)	0.0026-0.400	0.023 - 0.500	
Detector	aviex	EIGER-4M	EIGER-4M
Detector distance (m)	1.800	2.000	2.000
Exposure (s per image)	1.0/0.5	0.5/0.5	0.5/0.5
Column		Shodex KW402.5	
Flow rate (ml/min)		0.5	
Sample volume (µl)		80	
Sample concentration (mg/ml)	10	6	6
Temperature (K)		293	
Structural parameters			
R_g (Å) Guinier	30.3	27.4	30.0
R_g (Å) P(r)	30.9	28.0	30.6
D_{max} (Å)	93.1	96.5	104.8
Porod volume ($Å^3$)	67400	63600	73900
Molecular mass determination			
Theoretical MW (kDa)	49.7	42.1	42.1
Qp MW (kDa)	39.2	40.8	44.7
MoW MW (kDa)	30.6	46.3	49.8
Vc MW (kDa)	37.8	41.6	45.4
Data analysis software			
Data reduction		Foxtrot 3.5.10-3979	
Data analysis		ATSAS 3.0	

Table S5. Oligonucleotide sequences and use

Name	DNA sequence	Use
pSB1A3-F	TGCCACCTGACGTCTAAGAA	sequence confirmation
pSB1A3-R	ATTACCGCCTTTGAGTGAGC	
SEQ-T7-lac	TAATACGACTCACTATAGGGGAATTGTG	
SEQ-PBAD	ACGCTTTTTATCGCAACTCTCTACTG	
SEQ-15a-ORI	GCGTCAGATTTCGTGATGCTTG	
AraE-N-F	GCCACGCTCACAAACATGTTC	
VcA2_K24_HR	ACCTTCTGAATGCTGCTTAGCCTC	*higA2* point mutation through IVA
VcA2_K24E_F	CAGCATTCAGAAGGTGAACTTACTCTGAAAACACATCATGTG	
VcA2_T26_HR	AAGCTTACCTTCTGAATGCTGCTTAG	
VcA2_T26E_F	ATTCAGAAGGTAAGCTTGAACTGAAAACACATCATGTGAATGATG	
VcA2_T29_HR	CATCATGTGAATGATGTGGGTGAGTTG	
VcA2_T29E_F	CACATCATTCACATGATGTTCTTTCAGAGTAAGCTTACCTTCTG	
VcA2_E37_HR	ACCCACATCATTCACATGATGTGTTTTCAG	
VcA2_E37R_F	TGTGAATGATGTGGGTCGCTTGAACATCTCACCGGATGAAATC	
VcA2_V46_HR	AGTATTCGCGAGCAGTTCAATATGTC	
VcA2_V46R_F	CTGCTCGCGAATACTGCGGATTTCATCCGGTGAGATGTTC	
VcA2_V46K_F	CTGCTCGCGAATACTTTTGATTTCATCCGGTGAGATGTTC	
VcA2_N72_HR	TTCTAATGTGCGCGAAGACGTATG	
VcA2_N72R_F	TCGCGCACATTAGAACGCTGGGAACAAGGTC	
VcA2_N72Q_F	TCGCGCACATTAGAACAGTGGGAACAAGGTC	
VcA2_N72L_F	TCGCGCACATTAGAACTGTGGGAACAAGGTCGTAG	
VcA2_N72M_F	TCGCGCACATTAGAAATGTGGGAACAAGGTCGTAG	
VcA2_S78_HR	GTGCCAAATGGTCAAGCGGTC	
VcA2_S78T_F	TTGACCATTTGGCACGGTACGACCTTGTTCCCAG	
VcA2_S78N_F	TTGACCATTTGGCACGTTACGACCTTGTTCCCAG	
IVA_T29E_T26E_F2	CACATCATTCACATGATGTTCTTTCAGTTCAAGTTCACCTTCTGAATGCTG	
IVA_T26E_F2	ATTCAGAAGGTGAACTTGAACTGAAAACACATCATGTGAATGATG	
IVA_T26_R2	AAGTTCACCTTCTGAATGCTGCTTAG	
VcA2_T29_HR2	CATCATGTGAATGATGTGGGTCGCTTG	
IVA_DloopB2_F	GACGACGAGGAGGATGACTCAGCGATTATCTATTACTTTCTCGATGAAAAGAG	*higB2* loop substitution through IVA
IVA_DloopB2_R2	GTCATCCTCCTCGTCGTCAACTCGAATTTTTCGCAAACCGCCAG	
DNA45-Cy5-F	/5Cy5/-AATTCTTGCCATCTGTACGCTTGGTGCGTACACTTCCTATATGAA	P_{higba2} fragment for annealing and the analysis of protein-DNA binding
DNA45-Cy5-R	TTCATATAGGAAGTGTACGCACCAAGCGTACAGATGGTAAGAATT	
DNA45-F	AATTCTTGCCATCTGTACGCTTGGTGCGTACACTTCCTATATGAA	
DNA33-Cy5-F	/5Cy5/-TGCCATCTGTACGCTTGGTGCGTACACTTCCTA	
DNA33-Cy5-F	TGCCATCTGTACGCTTGGTGCGTACACTTCCTA	
DNA33-R	TAGGAAGTGTACGCACCAAGCGTACAGATGGCA	

Table S6. Homology region overhang sequences 5'-3' for Golden Gate cloning into pRAT-sfGFP-HigBA2

Homology region	Overhang (on vector)	Overhang (on insert)	insert
HR7	GAGC	GCTC	P_{CP8} *araE*
HR8	AGGA	TCCT	

Table S7. Minimal media composition

Component	c_0	c_K	V [mL]
M9 salts	10x	1x	50
glycerol	80%	4%	25
$MgSO_4$	1 M	1 mM	0.5
Trace elements solution	100x	1x	5
Water (miliQ)		to Σ	419.5
Σ			500 mL

M9 Salts	c_k [mM]	m [g]
$Na_2HPO_4x2H_2O$	422	37.7
KH_2PO_4	220	15
NaCl	85.6	2.5
NH_4Cl	67	2.5
Σ	water (miliQ) to 500 mL	

Trace elements solution	c_0 [M]	m [g]	c_k [mM]	V [mL]
$FeCl_2x6H_2O$		728	3.1	
$ZnCl_2$		84	0.62	
$CuCl_2x2H_2O$	0.1		$76*10^{-3}$	0.765
$CoCl_2x6H_2O$	0.2		$42*10^{-3}$	0.21
H_3BO_3	0.1		$162*10^{-3}$	1.6
$MnCl_2x4H_2O$	1		$8.1*10^{-3}$	0.0081
Water (miliQ)				
Σ				1000 mL

pH of Trace Elements Solution is adjusted to 7.5 using 1 M NaOH

Table S8. Parameters for the simulation of studied regulatory systems. Basic values are obtained from the article[27] for phd/doc module. Value of factor E is 1 if no repressor is bound to the operator (D=m) and 0 in any other case.

Parameter	Propensity	Normal simulation	Changed parameters	Units	Meaning
ζ	ζ*E	0.138375	0.138375	s^{-1}	mRNA transcription
ρ_A	ρ_A *mRNA	0.137	0.137/10	s^{-1}	Antitoxin translation
ρ_T	ρ_T *mRNA	0.053	0.053/10	s^{-1}	Toxin translation
dm	dm *mRNA	$1.70 \cdot 10^{-3}$	$1.70 \cdot 10^{-3}$	s^{-1}	mRNA degradation
dm_T	dm_T *mRNA*T	$1.0 \cdot 10^{-4}$	$1.0 \cdot 10^{-4}$	s^{-1}	Cleavage of mRNA by toxin
dA	dA *A	$1.155 \cdot 10^{-3}$	$1.155 \cdot 10^{-3} \cdot 8$	s^{-1}	Antitoxin degradation
dTA	dTA *TA and dTA *TAT	$2.310 \cdot 10^{-4}$	$2.310 \cdot 10^{-4} \cdot 8$	s^{-1}	Degradation of antitoxin inside TA and TAT complexes
dC	dC *TA and dC *TAT and dC*T	$2.8881 \cdot 10^{-4}$	$2.8881 \cdot 10^{-4}/10$	s^{-1}	Degradation of toxin and both complexes (TA and TAT)
α_C	α_C*A*T and α_C*TA*T	0.0234	0.0234	s^{-1}	Formation of complexes
θ_C	θ_C*TA and θ_C*TAT	$5.3 \cdot 10^{-5}$	$5.3 \cdot 10^{-5}$	s^{-1}	Dissociation of complexes
K_C	α_C/ θ_C	442	442		Association constant for complex formation
α_A	α_A*D*repressor	$2.665 \cdot 10^{-5}$	$2.665 \cdot 10^{-5}$	s^{-1}	Binding to operator
θ_A	θ_A*(m-D)	$2.8875 \cdot 10^{-3}$	$2.8875 \cdot 10^{-3}$	s^{-1}	Unbinding from operator
K_d	α_A/ θ_A	$9.229 \cdot 10^{-3}$	$9.229 \cdot 10^{-3}$		Association constant for DNA binding
m		1	1		Number of binding sites

Supplementary Figures

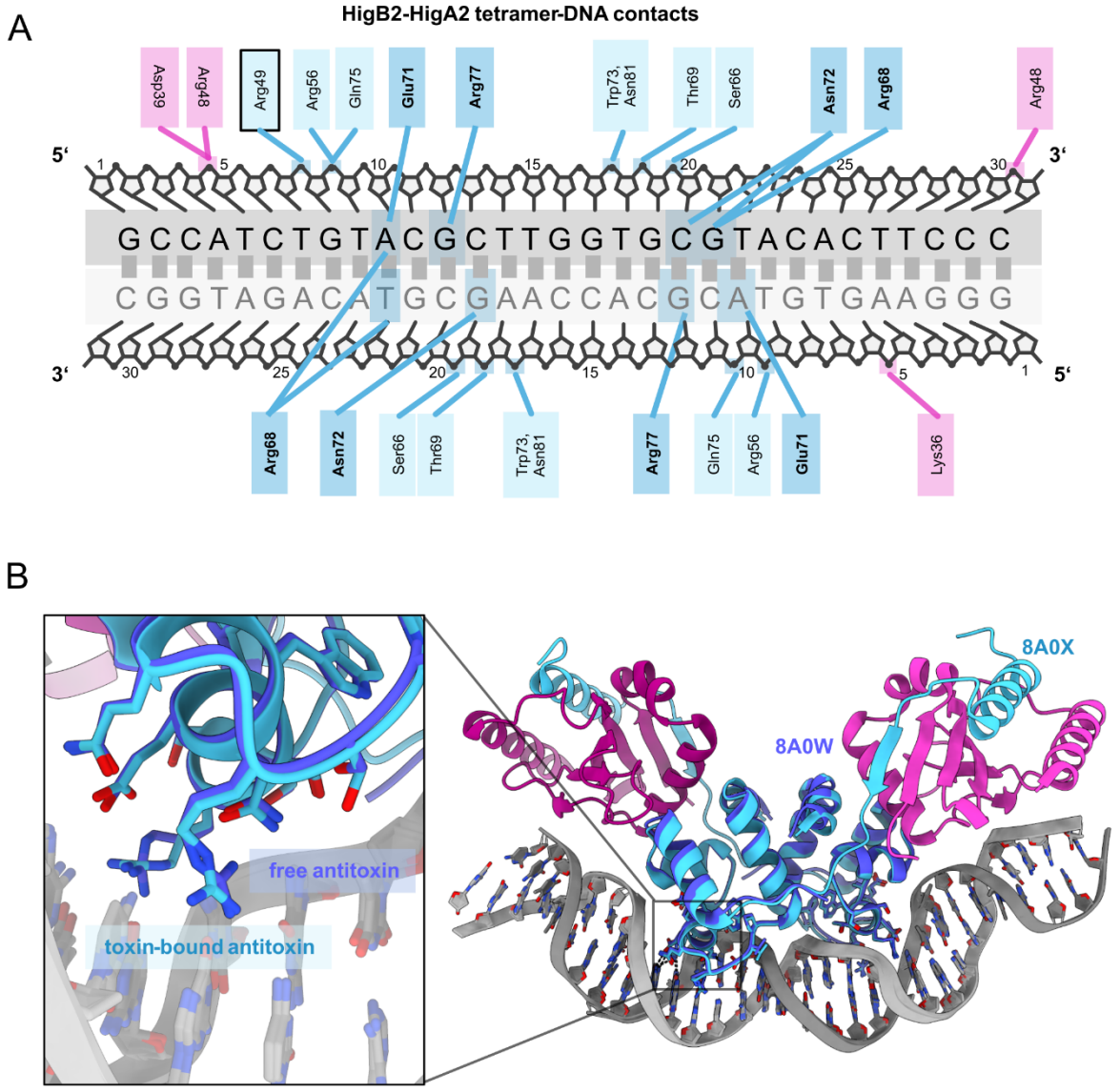

Figure S1. Comparison of antitoxin DNA-binding as antitoxin dimer HigA2 versus toxin-bound tetramer HigB2-HigA2. A. Schematic representation of antitoxin-DNA contacts in the DNA-bound HigB2-HigA2 tetramer (determined from crystal cstructure PDBID:8A0X). Blue and pink boxes represent antitoxin and toxin amino acids, respectively. Bold outline represents novel antitoxin interaction not determined from antitoxin alone bound to DNA (PDBID: 8A0W). Amino acids depicted in bold represent base-pair binding residues. **B.** Structural comparison of antitoxin dimer (dark blue, PDBID: 8A0W) bound to DNA and toxin-antitoxin tetramer (light blue, light/dark pink, PDBID: 8A0X). Inset depicts a closeup comparison of amino acid orientations in the DNA-binding region.

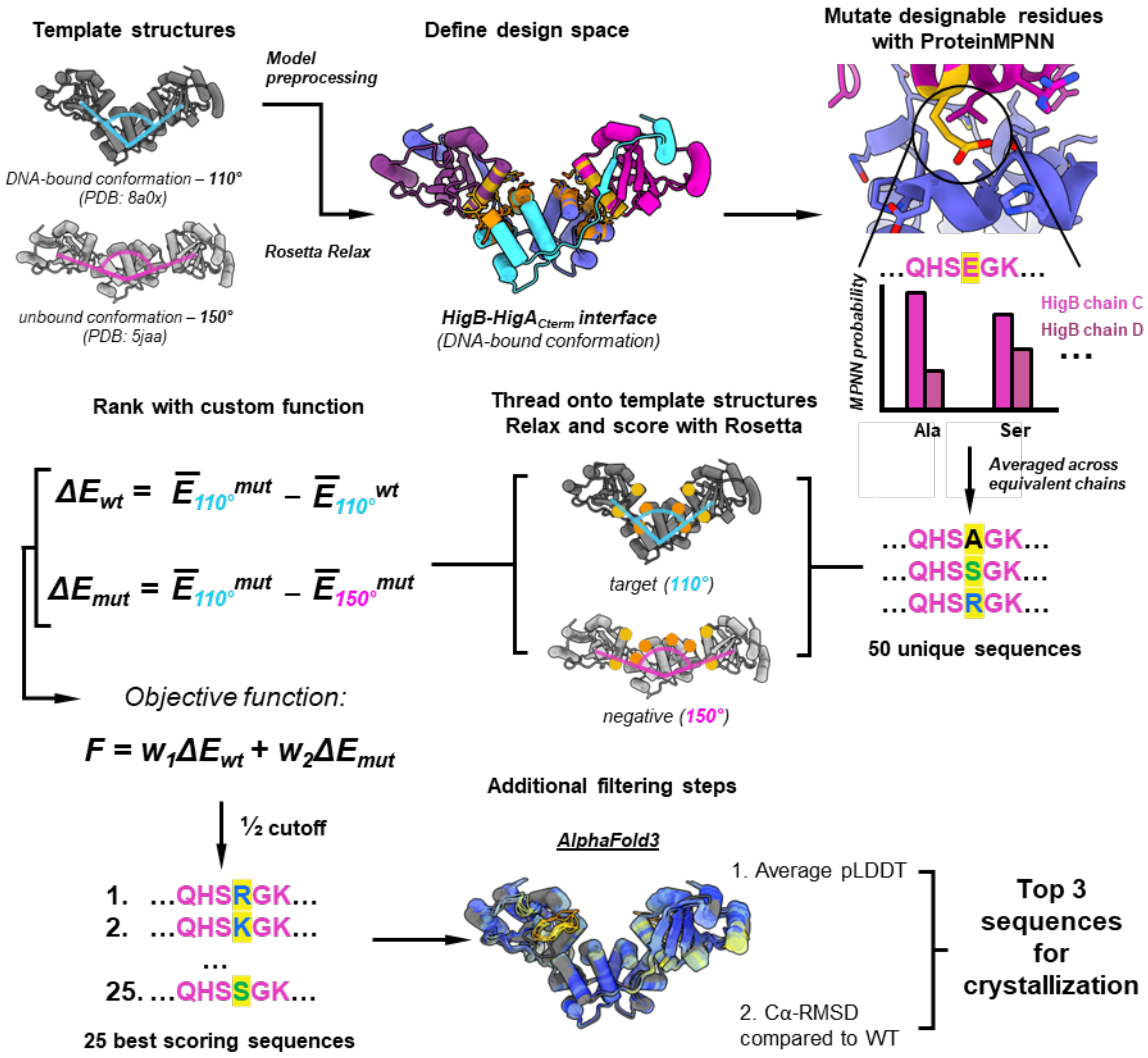

Figure S2. ***In silico*** **pipeline for design of conformationally constrained variants HigB2-A2$_{110A-C}$.**

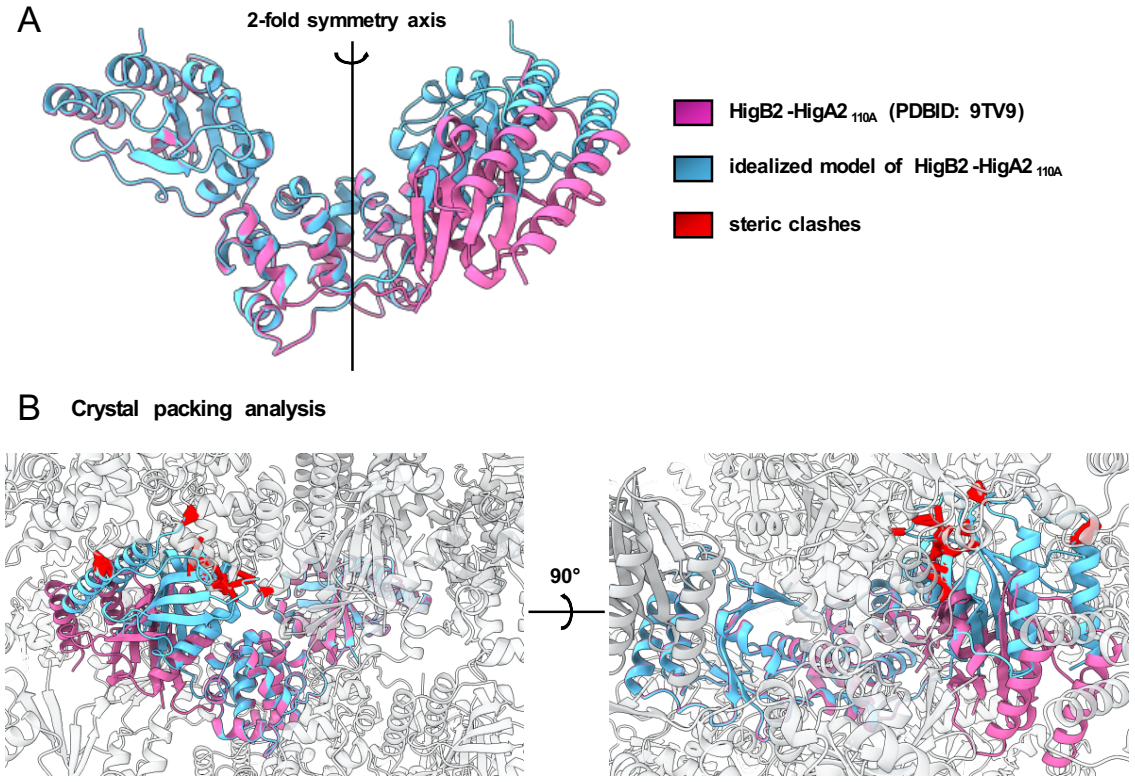

Figure S3. Analysis of crystal packing in the V-shaped HigB2-HigA2$_{110A}$ x-ray structure. A. Superposition of the HigB2-HigA2$_{110A}$ crystal structure (pink) and an idealized symmetric model (blue). The symmetric model was built by generating a duplicate of the HigB2-HigA2 pair with lower RMSD to the AlphaFold3 prediction of the designed sequence, which was rotated across the twofold symmetry axis of the HigA2 C-terminal domain. **B.** Crystal packing profile of HigB2-HigA2$_{110A}$ with the superimposed idealized symmetric model. Steric clashes are shown in red. The difference in orientation between the two HigB2 units in the HigB2-HigA2$_{110A}$ crystal structure can be explained by its crystal packing profile. Crystal packing was assessed by generating symmetry mates of the HigB2-HigA2$_{110A}$ crystal structure within a distance of 4 Å in ChimeraX, and the idealized symmetric model was superimposed onto the HigA2 C-terminal dimer of the original HigB2-HigA2$_{110A}$ crystal structure. Steric clashes with neighbouring symmetry mates were computed for both models as all pairs of heavy atoms with a vdW radius overlap > 0.60 Å, correcting for H-bonds by subtracting 0.40 Å.

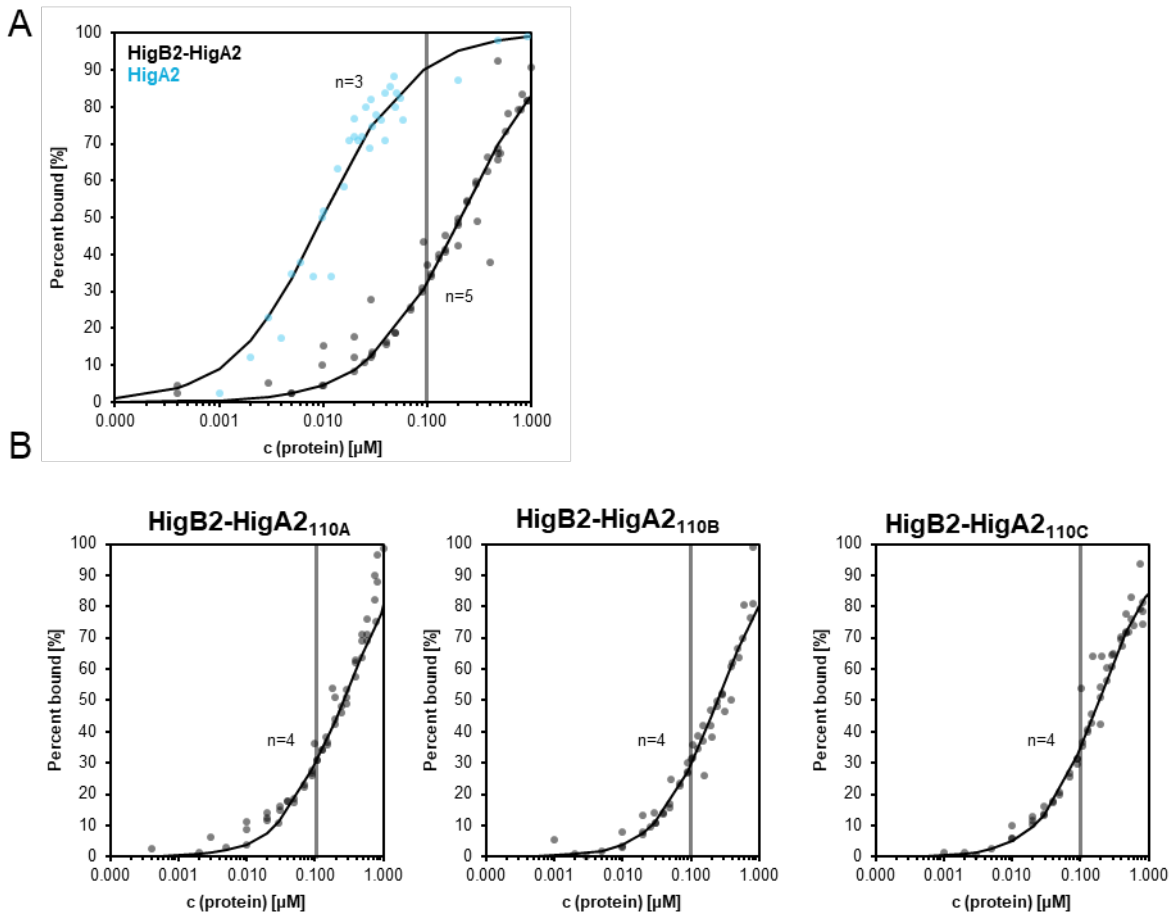

Figure S4. Fluorescence anisotropy measurements comparing DNA-binding of A. HigA2 (blue), HigB2-HigA2 (black), B. HigB2-HigA2$_{110A}$ (left), HigB2-HigA2$_{110B}$ (middle) and HigB2-HigA2$_{110C}$ (right) to DNA45-Cy5 probe. Global fit of model function is depicted as a solid black line. Gray line represents 0.1 µM protein concentration.

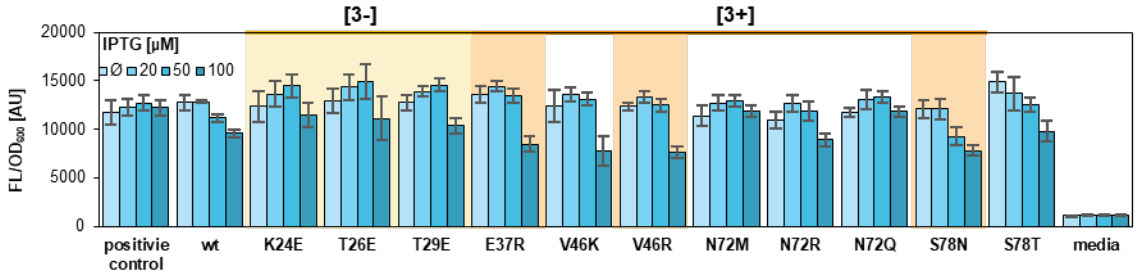

Figure S5. In vivo repression scan of single-residue mutations through normalized fluorescence measurements (FL/OD$_{600}$) of cells expressing IPTG-inducible HigA2 and its variants in increasing concentrations of IPTG at 10 h post induction. Select binding-enhancing and binding-disrupting mutants are depicted in orange and yellow, respectively.

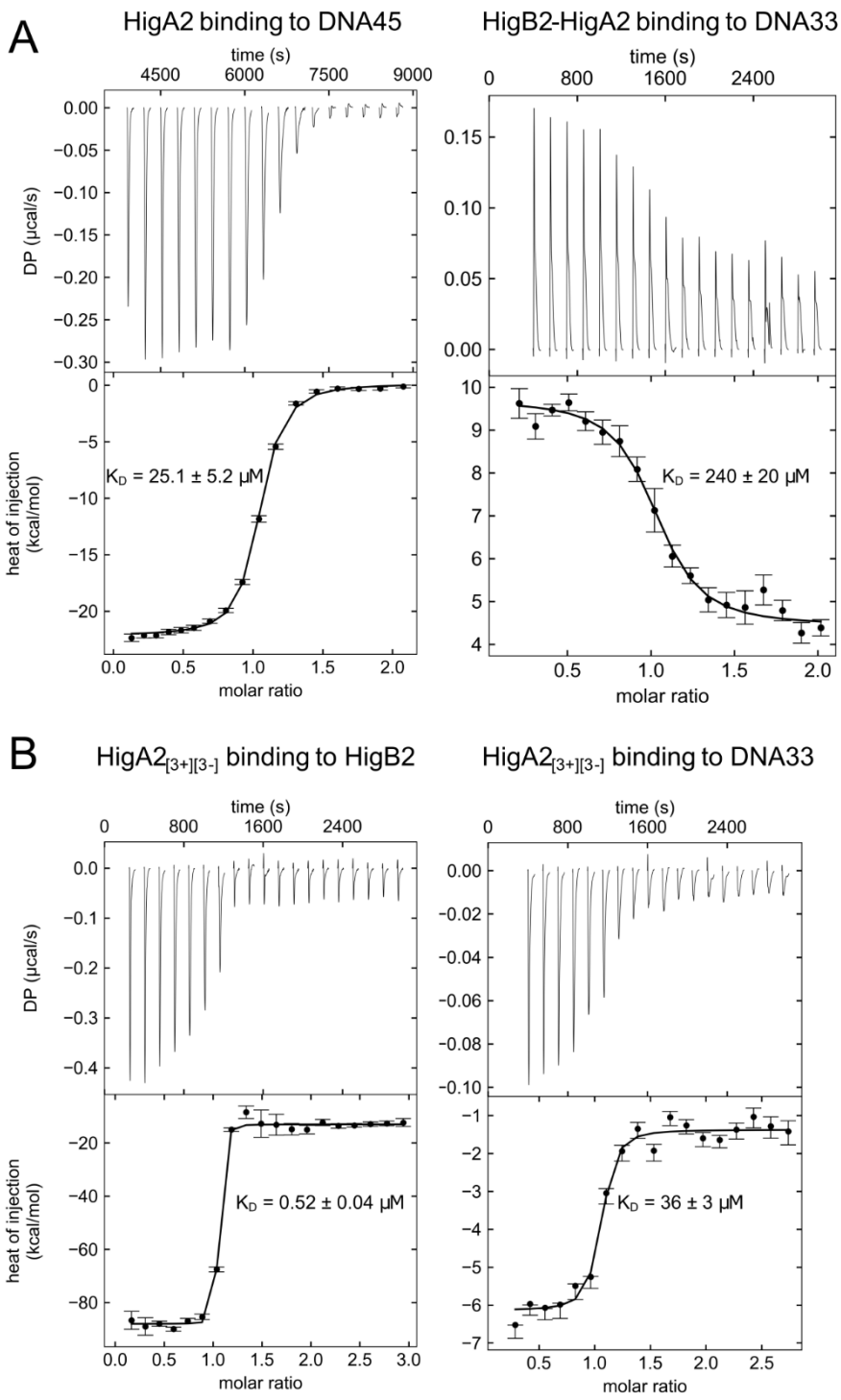

Figure S6. ITC binding curves. A. Binding curves of HigA2 (left) and HigB2-HigA2 (right) to operator DNA33. **B.** Binding curves of $HigA2_{[+][-]}$ to HigB2 (left) and DNA33 (right).

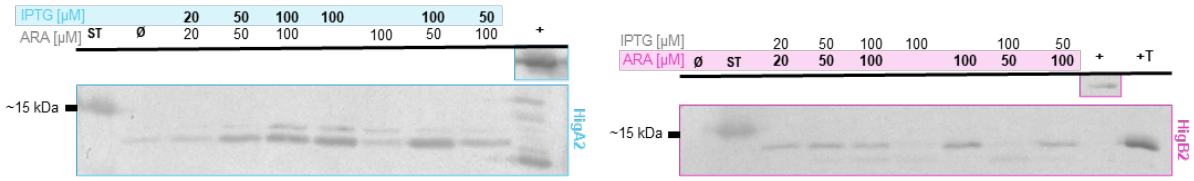

Figure S7. Western blot analysis following HigB2 (pink, right) and HigA2 (blue, left) purification though His- and HA-tag, respectively. IPTG and L-arabinose (ARA) concentrations are highlighted and denoted in bold when detecting the protein induced. Images have been cropped for easier analysis. His-GST-HA (+) has been added as a positive control. For the analysis of HigB2, purified His-tagged HigB2 (+T) has also been added.

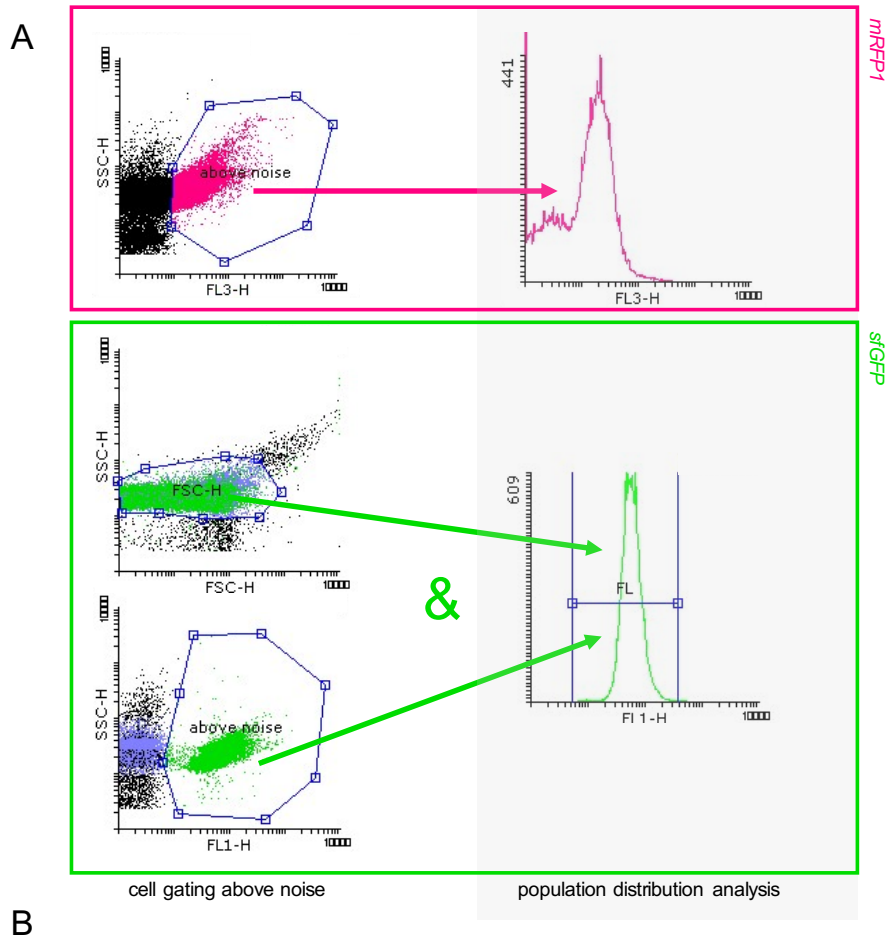

Figure S8. Cell gating example of flow cytometry experiments (A) and flow cytometry data of cells expressing *sfGFP* from pRAT-sfGFP-*higB/higA*(B). A. Events above a certain level of noise likely representing cells are selected and denoted in pink (*mRFP1*) and green (*sfGFP*) for experiments involving constitutive and inducible promoters, respectively. **B.** Single cell population distribution of cells expressing *sfGFP* preceded by P_{higBA2} promoter on vector pRAT-sfGFP-HigBA2 following 20 h growth without inducer (white), with 100 µM IPTG (blue), 100 µM arabinose (pink) or both (purple). Three colonies of each experimental setup were measured (n=3).

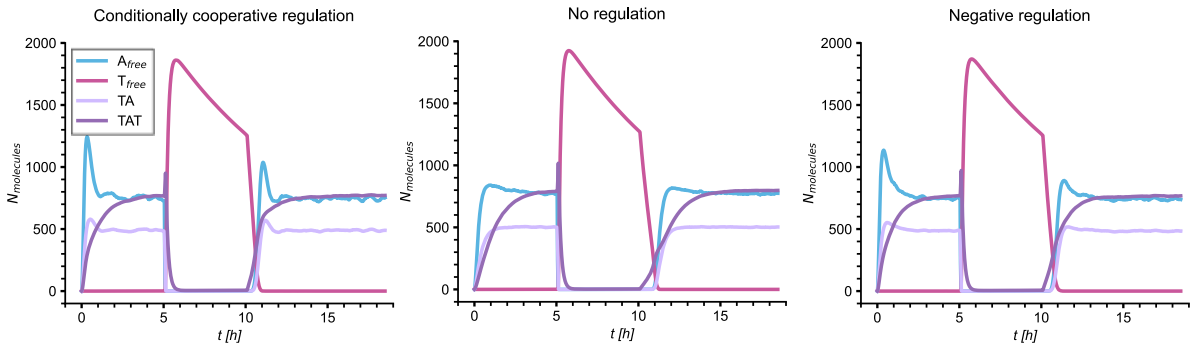

Figure S9. Simulated molecule distribution of different regulation mechanism in response to stress (starvation). The blue line represents free antitoxin (A_{free}), pink line represents free toxin (T_{free}) and purple lines represent toxin-antitoxin complexes (TA-light purple, TAT-purple).

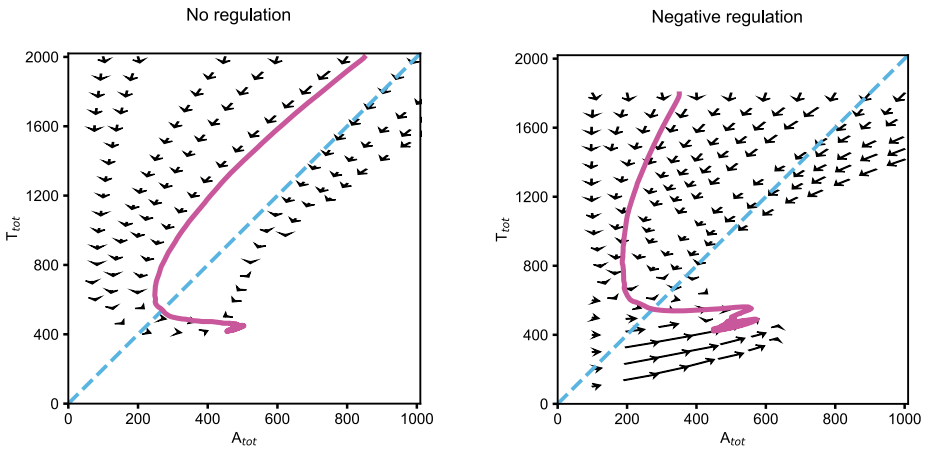

Figure S10. Vector Fields of TA systems with five binding sites on the operator. On the left is the vector field for simulation without regulation and on the right is the vector field for simulation with negative regulation. Simulations were made comparable by achieving same steady-state levels either by the change in level of repression (negative regulation: αA/3 and θA*3) or by reduced mRNA production (ζ/ 4.9 and dm *4.9). Pink lines are the trajectories that intersect the diagonal line (Ttot:Atot=2:1) at the same point in both simulations. Length of individual arrows represent the rate of change of Atot and Ttot in the system.

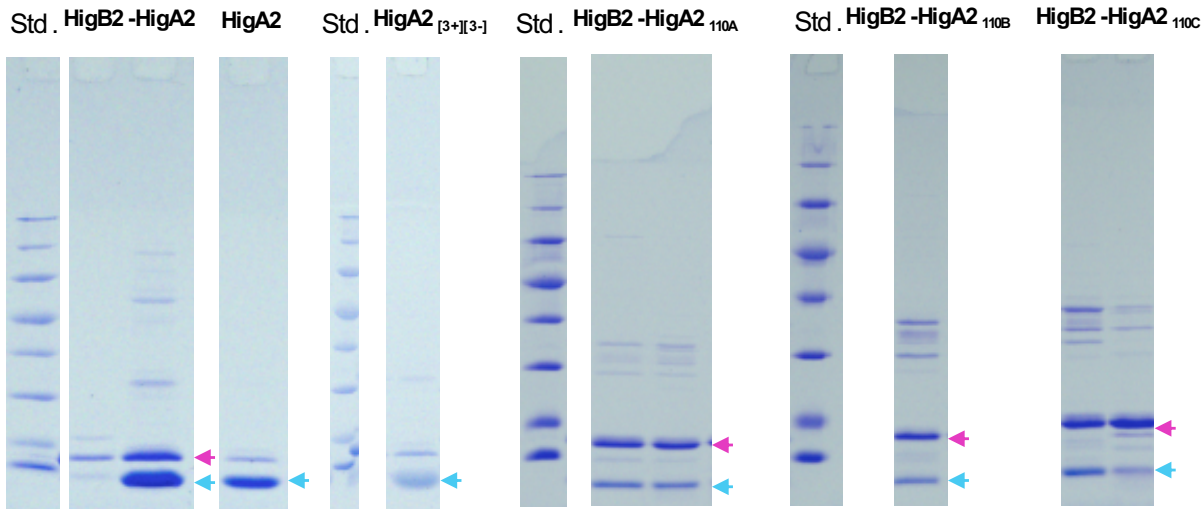

Figure S11. Examples of SDS-PAGE of purified proteins. Bands representing toxin and antitoxin are marked with pink and blue arrow, respectively. Unstained MW marker is denoted as Std. Images are cropped for convenience.

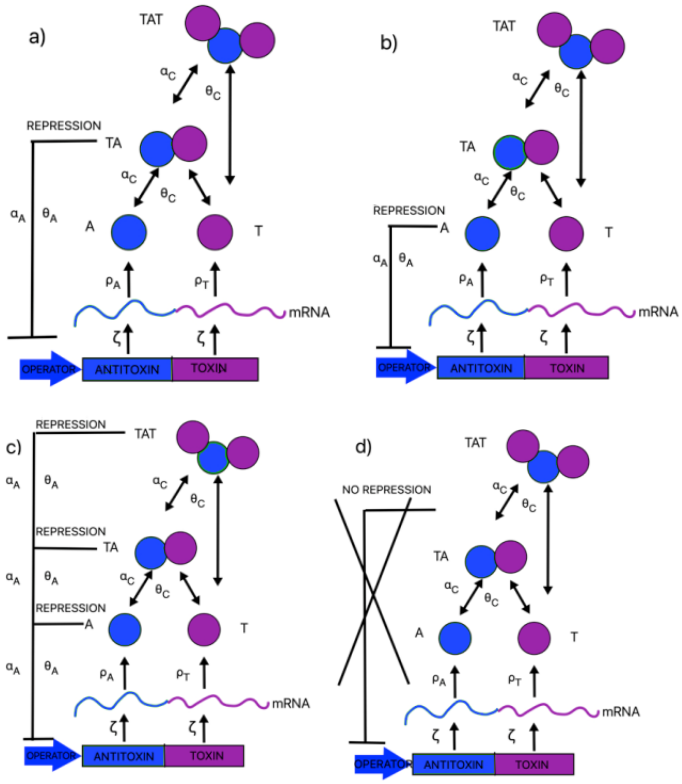

Figure S12. Schematic representation of four different regulatory systems: a) conditional cooperative regulation, b) anti-cooperative regulation, c) negative regulation, and d) no regulation.

References

1. Bikard, D. *et al.* Programmable repression and activation of bacterial gene expression using an engineered CRISPR-Cas system. *Nucleic Acids Res.* **41**, 7429–7437 (2013).

2. Živič, Z., Lipoglavšek, L., Lah, J. & Hadži, S. A single vector system for tunable and homogeneous dual gene expression in Escherichia coli. *Sci. Rep.* **15**, 99 (2025).

3. Engler, C. & Marillonnet, S. Golden Gate Cloning. in 119–131 (2014). doi:10.1007/978-1-62703-764-8_9.

4. Bird, J. E., Marles-Wright, J. & Giachino, A. A User's Guide to Golden Gate Cloning Methods and Standards. *ACS Synth. Biol.* **11**, 3551–3563 (2022).

5. García-Nafría, J., Watson, J. F. & Greger, I. H. IVA cloning: A single-tube universal cloning system exploiting bacterial In Vivo Assembly. *Sci. Rep.* **6**, 27459 (2016).

6. Green, M. R. & Sambrook, J. The Inoue Method for Preparation and Transformation of Competent *Escherichia coli*: "Ultracompetent" Cells. *Cold Spring Harb. Protoc.* **2020**, pdb.prot101196 (2020).

7. Sterckx, Y. G.-J. *et al.* An efficient method for the purification of proteins from four distinct toxin–antitoxin modules. *Protein Expr. Purif.* **108**, 30–40 (2015).

8. Serhii Hirka & Maureen McKeague. Quantification of aptamer-protein binding with fluorescence anisotropy. *Aptamers* **5**, 1–6 (2021).

9. Scheuermann, T. H. & Brautigam, C. A. High-precision, automated integration of multiple isothermal titration calorimetric thermograms: New features of NITPIC. *Methods* **76**, 87–98 (2015).

10. Zhao, H., Piszczek, G. & Schuck, P. SEDPHAT - A platform for global ITC analysis and global multi-method analysis of molecular interactions. *Methods* **76**, 137–148 (2015).

11. Hadži, S., Garcia-Pino, A., Gerdes, K., Lah, J. & Loris, R. Crystallization of two operator complexes from the Vibrio cholerae HigBA2 toxin-antitoxin module. *Acta Crystallogr. F Struct. Biol. Commun.* **71**, 226–233 (2015).

12. Hadži, S. *et al.* Crystallization of the HigBA2 toxin–antitoxin complex from *Vibrio cholerae*. *Acta Crystallogr. Sect. F Struct. Biol. Cryst. Commun.* **69**, 1052–1059 (2013).

13. Emsley, P., Lohkamp, B., Scott, W. G. & Cowtan, K. Features and development of Coot. *Acta Crystallogr. D Biol. Crystallogr.* **66**, 486–501 (2010).

14. Adams, P. D. *et al. PHENIX*: a comprehensive Python-based system for macromolecular structure solution. *Acta Crystallogr. D Biol. Crystallogr.* **66**, 213–221 (2010).

15. David, G. & Pérez, J. Combined sampler robot and high-performance liquid chromatography: A fully automated system for biological small-angle X-ray scattering experiments at the Synchrotron SOLEIL SWING beamline. *J. Appl. Crystallogr.* **42**, 892–900 (2009).

16. Petoukhov, M. V. *et al.* New developments in the ATSAS program package for small-angle scattering data analysis. *J. Appl. Crystallogr.* **45**, 342–350 (2012).

17. Bakan, A., Meireles, L. M. & Bahar, I. ProDy: Protein Dynamics Inferred from Theory and Experiments. *Bioinformatics* **27**, 1575–1577 (2011).

18. Dauparas, J. *et al.* Atomic context-conditioned protein sequence design using LigandMPNN. *Nature Methods 2025 22:4* **22**, 717–723 (2025).

19. Leaver-Fay, A. *et al.* Rosetta3: An Object-Oriented Software Suite for the Simulation and Design of Macromolecules. *Methods Enzymol.* **487**, 545–574 (2011).

20. Fleishman, S. J. *et al.* RosettaScripts: a scripting language interface to the Rosetta macromolecular modeling suite. *PLoS One* **6**, (2011).

21. Havranek, J. J., Duarte, C. M. & Baker, D. A simple physical model for the prediction and design of protein-DNA interactions. *J. Mol. Biol.* **344**, 59–70 (2004).

22. Ashworth, J. *et al.* Computational redesign of endonuclease DNA binding and cleavage specificity. *Nature* **441**, 656 (2006).

23. Thyme, S. & Song, Y. Computational Design of DNA-Binding Proteins. *Methods in Molecular Biology* **1414**, 265–283 (2016).

24. Meng, E. C. *et al.* UCSF ChimeraX: Tools for structure building and analysis. *Protein Sci.* **32**, e4792 (2023).

25. Stein, A. & Kortemme, T. Improvements to Robotics-Inspired Conformational Sampling in Rosetta. *PLoS One* **8**, e63090 (2013).

26. Pavlovicz, R. E., Park, H. & DiMaio, F. Efficient consideration of coordinated water molecules improves computational protein-protein and protein-ligand docking discrimination. *PLoS Comput. Biol.* **16**, e1008103 (2020).

27. Hubbard, S. J. & Thornton, J. NACCESS: program for calculating accessibilities. *Department of Biochemistry and Molecular Biology, University College of London* (1992).

28. Dauparas, J. *et al.* Robust deep learning-based protein sequence design using ProteinMPNN. *Science* **378**, 49–56 (2022).

29. Abramson, J. *et al.* Accurate structure prediction of biomolecular interactions with AlphaFold 3. *Nature 2024 630:8016* **630**, 493–500 (2024).

30. Vandervelde, A. *et al.* Molecular mechanism governing ratio-dependent transcription regulation in the ccdAB operon. *Nucleic Acids Res.* **45**, 2937–2950 (2017).

31. Bois, J. & Elowitz, M. Stochastic simulation of biological circuits. *Caltech* http://be150.caltech.edu/2019/handouts/12_stochastic_simulation_all_code.html (2019).

32. Cataudella, I., Trusina, A., Sneppen, K., Gerdes, K. & Mitarai, N. Conditional cooperativity in toxin–antitoxin regulation prevents random toxin activation and promotes fast translational recovery. *Nucleic Acids Res.* **40**, 6424–6434 (2012).

33. Gelens, L., Hill, L., Vandervelde, A., Danckaert, J. & Loris, R. A General Model for Toxin-Antitoxin Module Dynamics Can Explain Persister Cell Formation in E. coli. *PLoS Comput. Biol.* **9**, e1003190 (2013).